



HAL
open science

Thermal shock resistance of a NiCrAlY-coated alloy 625 system produced by laser powder bed fusion

Mathieu Ternier, Jiwon Lee, Baptiste Ruggieri, Etienne Copin, Oxana Ostrovskaya, Claudio Badini, Philippe Lours, Hyun-Uk Hong

► To cite this version:

Mathieu Ternier, Jiwon Lee, Baptiste Ruggieri, Etienne Copin, Oxana Ostrovskaya, et al.. Thermal shock resistance of a NiCrAlY-coated alloy 625 system produced by laser powder bed fusion. *Surface and Coatings Technology*, 2021, 417, pp.1-14/127217. 10.1016/j.surfcoat.2021.127217 . hal-03211765

HAL Id: hal-03211765

<https://imt-mines-albi.hal.science/hal-03211765>

Submitted on 7 May 2021

HAL is a multi-disciplinary open access archive for the deposit and dissemination of scientific research documents, whether they are published or not. The documents may come from teaching and research institutions in France or abroad, or from public or private research centers.

L'archive ouverte pluridisciplinaire **HAL**, est destinée au dépôt et à la diffusion de documents scientifiques de niveau recherche, publiés ou non, émanant des établissements d'enseignement et de recherche français ou étrangers, des laboratoires publics ou privés.

Thermal shock resistance of a NiCrAlY-coated Alloy 625 system produced by Laser Powder Bed Fusion

Mathieu Terner¹, Jiwon Lee^{1,2}, Baptiste Ruggieri², Etienne Copin^{2*}, Oxana Ostrovskaya³, Claudio Badini³, Philippe Lours², Hyun-Uk Hong¹

¹ Department of Materials Convergence and System Engineering, Changwon National University, 20 Changwondaehak-ro, Changwon, Gyeongnam 51140, Korea

² Institut Clément Ader (ICA), Université de Toulouse, CNRS, IMT Mines Albi, INSA, ISAE-SUPAERO, UPS, Campus Jarlard, F-81013 Albi, France

³ Department of Applied Science and Technology, Politecnico di Torino, Corso Duca degli Abruzzi 24, 10129 Torino, Italy

*Corresponding author: Etienne Copin (etienne.copin@mines-albi.fr), IMT Mines Albi Campus Jarlard 81013 Albi CT Cedex 09 France, tel: +33 5 63 49 30 74, fax: +33 5 63 49 30 99

Abstract

Additive Manufacturing offers an innovative route for producing high-quality parts in various fields. A bi-material system, consisting in a NiCrAlY bond coat deposited onto a Ni-based Alloy 625 substrate, was manufactured by laser powder bed fusion (LPBF). Test samples were prepared and included SolGel ceramic $ZrO_2(Y_2O_3)$ top coats as well as a specific grain boundary serration (GBS) heat treatment for promoting high temperature resistance. These specimens were subjected to very severe thermal shock cycles between 950 °C and 300 °C, characterized by steep heating and air quenching rates in a state-of-the-art burner rig designed to render gas turbine conditions, and their integrity was compared. While LPBFed NiCrAlY coatings were relatively spared from degradations due to thermal shocks, ceramic top coats exhibited clear spallation. Poor bonding

was particularly experienced by specimens subjected to the GBS heat treatment due to the unavoidable formation therein of surface oxides. Numerous cracks were detected within NiCrAlY bond coats, both in tested specimens as well as in pre-cycled as-built ones, which suggested a dominant role of the LPBF process known for generating residual stress. Heat treated specimens exhibited nearly no cracking. Hardness was found to significantly increase within as-built NiCrAlY bond coats as a result of heat exposure during thermal shock cycling and was attributed to precipitations. The fully recrystallized microstructure of heat treated specimens, on the other hand, was found more stable. The present study completes a series of investigations demonstrating the great potential for manufacturing excellent high temperature structural components by means of LPBF as opposed to more constraining conventional routes.

Keywords: Additive manufacturing; laser powder bed fusion; thermal barrier coating; superalloy; thermal shock; microstructure;

1. Introduction

Additive Manufacturing is leading the fourth industrial revolution as an outstanding alternative to conventional manufacturing methods. Laser powder bed fusion (LPBF) in particular has emerged for more than a decade as an exceptional opportunity to produce certain metals otherwise challenging to manufacture by conventional deformation or solidification routes. This relatively new process rises numerous challenges in terms of metallurgy, microstructure and properties of materials produced. A large number of studies reported successful production of metallic alloys exhibiting close to full density and mechanical properties favorably comparable to their conventional counterparts [1]. In a recent publication, the innovative fabrication by LPBF of a bi-material system had been investigated, namely a NiCrAlY bond coat deposited onto a nickel-

based Alloy 625 substrate for high temperature applications [2]. The optimization of the process parameters for producing the bond coat directly onto the substrate, also produced by LPBF, focused on density and microstructure. This was the first time that such a production of this bi-material system had been reported. In particular, the results of the previous investigation suggested excellent adhesion of the bond coat onto the substrate due to the peculiar nature of the LPBF process involving partial remelting of underlying material, generating what was defined as a dilution zone. This contrasted with conventional deposition techniques, such as atmospheric plasma spray (APS) or electron beam physical vapor deposition (EB-PVD), which usually exhibit clear and well-defined interface between substrates and bond coats [3,4]. Promoting further bonding through interdiffusion requires long heat treatments at elevated temperatures [5].

The successful manufacturing of the NiCrAlY-Alloy 625 system produced by LPBF is predicated on the thorough characterization of the materials system behavior, particularly in terms of mechanical and environmental properties. For this reason, a series of investigations reported the typical as-built microstructure and its optimization by means of post processing heat treatment, as well as mechanical and oxidation behavior at elevated temperatures [6,7]. The experimental results suggested that LPBF offers an attractive alternative approach for manufacturing the bi-material system, which exhibited excellent properties often superior to those of conventional systems (wrought Alloy 625 and sprayed NiCrAlY). As hinted previously, this material system consists in a popular superalloy substrate attractive for its outstanding mechanical properties combined with a Ni-based Al-rich bond coat (NiCrAlY) to provide heat insulation and improve oxidation resistance. Intermediate bond coats are often more generally used to accommodate thermal expansion differences between the superalloy substrate and an outer ceramic top coat as part of so-called thermal barrier coating (TBC) systems [3,4]. TBCs are most commonly used to enhance high temperature applicability of superalloys in oxidizing and corrosive environments

specifically for gas turbine structural components for aeroengines and power generation. These components are in particular subjected to severe thermal cycles in operation which cause cracking, delamination and possible spallation of the TBC therefore reducing life of the components in operation [3,4].

The present study investigates the response of the NiCrAlY-Alloy 625 system produced by LPBF when subjected to aggressive thermal cycles and thermal shocks. A state-of-the-art burner rig specifically designed to simulate gas turbine engines environment was used to impose short, frequent and sharp thermal cycles in air between 600 and 950 °C to test specimens. A Zr-rich top coat was also deposited by conventional SolGel process and a specific heat treatment for promoting grain boundary serration [6] was applied beforehand to reproduce conditions close to that of a typical TBC system.

2. Materials and methods

2.1 Raw Materials and LPBF processing

Gas-atomized Alloy 625 powder suitable for LPBF production was provided by the machine manufacturer (SLM Solutions). A SLM 125HL was used for the fabrication of test specimens and followed the procedure described in [2,6,7]. A stripe scanning strategy with a 33° rotation between layers was used and default optimal parameter conditions for Alloy 625 were utilized (laser power $P = 275$ W, scanning speed $v = 760$ mm/s, hatching distance $h = 120$ μm and layer thickness $t = 50$ μm). These conditions led to low residual porosity levels measured below 0.1 %. Nine cylindrical specimens with a diameter of 22 mm and a length of 22 mm were built vertically onto the superalloy building platform. After production of the Alloy 625 substrate samples, the machine was thoroughly cleaned and the powder was changed into NiCrAlY. The platform was

carefully levelled so that the zero position would match the substrate surface for processing of the NiCrAlY coatings directly onto the Alloy 625 substrates. The empty volume was filled with powders to complete the powder bed. It should be noted that no surface treatment or heat treatment was applied to the LPBFed Alloy 625 substrate samples prior to processing of the NiCrAlY coatings.

Unconventional gas atomized NiCrAlY pre-alloyed powder with characteristics appropriate for LPBF processing was specially delivered by Ducal International. The LPBF processing conditions for depositing the bond coat derived from the optimization campaign described in [2]. Optimum processing conditions were then determined to be laser power $P = 250$ W, scanning speed $v = 800$ mm/s, hatching distance $h = 120$ μm and layer thickness $t = 50$ μm as well as a 67° rotation between layers [2,7]. Two 50 μm NiCrAlY coating layers were built onto the substrates. Given the apparent density of the powder (approximately 60%) this theoretically corresponds to a coating thickness of about 70 μm , which is close to the typical thickness of MCrAlY bond coats in TBC systems [3]. The effective thickness of the bond coat was however larger due to the dilution zone mentioned earlier [2,7]. Nine NiCrAlY-coated Alloy 625 cylindrical specimens were produced. The chemical compositions of the starting powders were measured by inductively coupled plasma optical emission spectroscopy (ICP-OES) and are given in Table 1. The selected LPBF process parameters for the production of specimens are given in Table 2.

Table 1: Chemical composition in wt. % measured by ICP-OES of Alloy 625 and NiCrAlY pre-alloyed powders used for LPBF manufacturing.

	Ni	Cr	Mo	Fe	Co	C	Nb	Al	Y
Alloy 625	Bal.	20.08	8.27	3.49	0.6	0.08	3.12	0.35	-
NiCrAlY	Bal.	22.01	-	-	-	-	-	9.34	1.165

Table 2: Process parameters for the production of Alloy 625 substrate and NiCrAlY bond coat by

LPBF

LPBF process parameters	Substrate Alloy 625	Bond coat NiCrAlY
Laser power P (W)	275	200
Scanning speed v (mm/s)	760	800
Hatching distance d (μm)		120
Layer thickness t (μm)		50

2.2 Heat treatment and ceramic coating

Three specimens were subjected to a specifically designed heat treatment intended to promote grain boundary serration. The grain boundary serration heat treatment was designed to enhance the high temperature mechanical properties of the LPBFed Alloy 625 substrate [6]. It consisted in heating as-built material to 1300 °C for 90 minutes followed by slow cooling at the controlled cooling rate of 5 °C/min down to the aging temperature of 870 °C at which the material was maintained for 2 h before air cooling to room temperature. This heat treatment was conducted in a sealed programmable tubular furnace (Nabertherm) under protective argon flow (75 l/hour) to provide inert atmosphere.

A ceramic coating was deposited onto the surface of the heat treated specimens, as well as three other as-built samples. This ceramic coating consisted in yttria-stabilized zirconia ($\text{ZrO}_2(\text{Y}_2\text{O}_3)$) deposited by air-spraying following a conventional SolGel process adapted from [8,9]. 8 mol% Y_2O_3 stabilized zirconia powder (TZ-8Y, Tosoh) was dispersed into a YSZ sol, and the resulting composite sol was air-sprayed onto the substrates in several passes. To promote bonding and

consolidate the coatings, a heat treatment was applied after deposition. It was carried out at an appropriately low temperature (600 °C) for 4h in order to avoid any significant evolution of the microstructure. The average thickness measured shortly after processing by an eddy-current based coating thickness meter (ISOSCOPE Fischer model FMP10) was consistent between 137 and 161 μm on average for all six specimens (average standard deviation of 20 μm). While the sol-gel route was selected at the time of the present study for its availability, more standard technologies such as APS or EB-PVD could be preferred in future research.

All nine specimens therefore consisted in: *i*) three as-built NiCrAlY-coated Alloy 625 (AB), *ii*) three as-built NiCrAlY-coated Alloy 625 with ceramic top coat (AB-TC) and *iii*) three NiCrAlY-coated Alloy 625 subjected to the grain boundary serration treatment and with ceramic top coat (GBS-TC). A schematic diagram of the different specimens and conditions is displayed in Figure 1.



Figure 1: Schematic diagram of the specimens produced by LPBF for thermal shock testing in burner rig

2.3 Thermal shock in burner rig

The NiCrAlY-coated Alloy 625 (+ top coat) is intended for use in high temperature exposure conditions such as aeroengine gas turbine applications. For this reason, resistance to thermal shock (rapid heating and cooling cycles) is critical. A state-of-the-art burner rig approaching the severe conditions was used to impose very rapid successive heating and cooling. This burner rig (Figure 2) is equipped with a combustion chamber consisting of a heat resistant ceramic plate machined to host up to 10 specimens, 20 air quenching tubes for fast cooling of the top and/or bottom surface of each specimens, 20 thermocouples for precise measurements of the temperature at the top and the bottom of each specimens. On top of the plate, a burner delivers an actual flame by burning either methane or a mixture of regulated methane + fuel. Only methane was used in the present study. A system of manual valves with manometer allows the regulation of the air flow rate for quenching (presently set to 10 m³/hour). The burner rig is controlled manually by means of a software which allows to regulate the methane flow and the air/methane ratio, trigger air quenching and monitor/control the temperatures. The maximum designed temperature is 1300 °C. In the present study, the methane flow was set to 1 m³/h and the air excess to 20 % with respect to the reaction stoichiometry to generate an oxidizing environment.

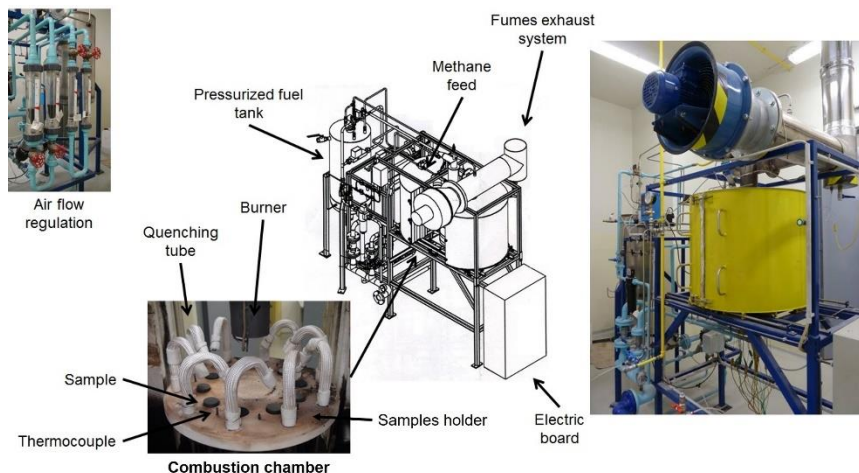


Figure 2: Burner rig hardware used for thermal shock testing

The test conditions for the materials were ideally the most representative of the severe conditions envisaged in operation. As many as 450 cycles were carried out under very aggressive conditions for the tested materials. Further cycling was avoided to prevent complete degradation of the ceramic top coat for analysis. With regards to the nature of the superalloy substrate (Alloy 625), a maximum temperature of 950 °C (2 min plateau) and quenching to 300 °C was considered. Note that 950 °C was the average temperature in the chamber calculated from six representative thermocouples. The actual temperature for each individual specimen varied significantly and was conveniently recorded. Nevertheless, the gradient of temperature was appropriately lower than 100 °C. Figure 3(a) shows the record of average temperature in the chamber for the entire 450 cycles carried out.

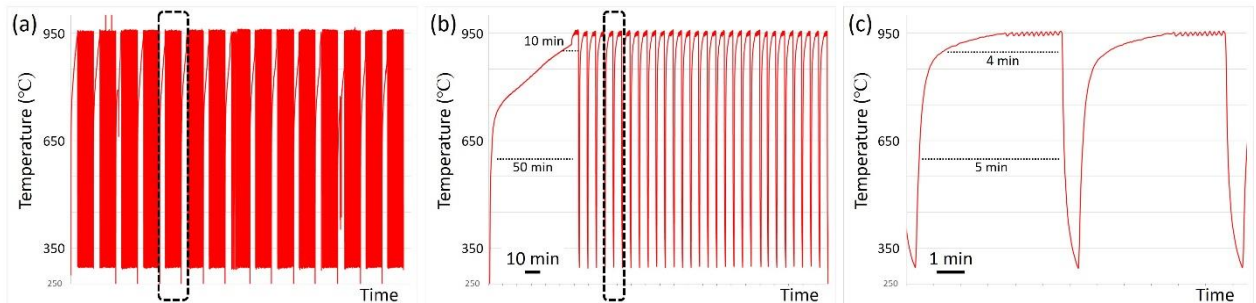


Figure 3: Average temperature measured inside the combustion chamber: (a) the whole 450 cycles, (b) a single uninterrupted 30-cycles session, and (c) details of two cycles between 300 and 950 °C

Fifteen 30-cycles sessions, each corresponding to one day of testing (approximately 4 hours continuously), are clearly observed in Figure 3(a). The burner rig is operated manually for safety considerations. The first heating of each 30-cycles session took approximately 1h because the

refractory ceramic combustion chamber was cold. Air quenching to 300 °C took only under 1 min and reheating to 950 °C took approximately 4 min (Figs 3(b) and 3(c)). After each session, the machine was cooled down and opened. Each sample was photographed and weighed with a precision balance, before being repositioned in the chamber for the next session on the next day. Slight maintenance of the machine was also necessary after each session to avoid in particular degradation of the quenching tubes (protected by glass-wool fabrics). As described earlier, three specimens were available for each of the three conditions (Figure 1). For each condition, one of these samples was not subjected to thermal cycling to maintain as-produced conditions for characterization (0 cycle), while the other two samples were conveniently placed diametrically opposed in the combustion chamber (Figure 2) to account for the variations in heat distribution.

2.4 Materials characterization

As mentioned in the previous section 2.3, each sample was photographed and weighed with a precision balance (KERN EW620-3NM, 1 mg precision) after each 30-cycles session to evaluate degradation of the specimens. Special care was systematically taken to avoid damaging the sensitive top coat during manipulations. After completion of the 450 thermal cycles, characterized by very rapid heating and cooling (Figure 3), each sample was protected by hot mounting the entire specimen within a phenolic conductive resin with carbon filler (Struers PolyFast) using an auto mounting press (MTDI MM-100). The specimens were then carefully sectioned in half along the building direction (along their length) between the front and the back of specimens with respect to the flame, with a precision cutting machine (Allied Techcut 5) equipped with a silicon carbide abrasive cut-off blade. The cutting operation was gentle with 2500 rpm rotation speed and low feed rate of $1.25 \text{ mm}\cdot\text{s}^{-1}$ together with abundant lubrication to

prevent damaging the TBC system as much as possible, in particular the brittle top coat. The specimens were subsequently ground using abrasive SiC papers from grit 400 to 2000 and polished using appropriate cloths and diamond pastes from 9 μm down to 1 μm . A number of analyses were performed prior to polishing with woven cloths and diamond pastes because these final polishing steps inevitably led to rip out of the brittle ceramic top coat, despite hot mounting intended for edge retention. Optical microscopy (OM, OLYMPUS BX51M) and Scanning Electron Microscopy (SEM, JSM-6510) equipped with energy dispersion X-ray spectroscopy (EDS) were utilized to analyze the materials. Electron backscattering diffraction (EBSD) with a field-emission scanning electron microscope (FE-SEM, MIRA-II) was also carried out to evaluate grain structure. To avoid artifacts from metallographic preparation, the final 1 μm polishing step was done using a colloidal silica suspension. Vickers microhardness (Mitutoyo HM-122) was measured every 20 μm from the top surface of the bond coat on 25 locations deep into the substrate for all conditions using a test load of 50 g. Three series of measurements were carried out: one at the center of the specimen, and one 5 mm away from the center on each side (flame side vs. furnace wall side).

3. Results and discussion

3.1 Mass gain and surface analysis

As mentioned in section 2.4, each sample was photographed and weighed after each 30-cycles session. Figure 4(a) shows the relative mass change in % for all six specimens tested as a function of the number of cycles. The top surface morphology evolution is included to appreciate in particular the degradation of the ceramic top coat (Figure 4(b)). A number of precautions must be considered before discussing results in Figure 4. First, while great care was taken, the procedure

described in section 2.3 includes moving manually each specimen from its location in the ceramic plate samples holder (Figure 2) for weighing and photographing before replacing it into the burner rig after slight maintenance when necessary. As a result, significant handling of the samples may inevitably alter the accuracy of measurements. Second, the initial weight of each sample was relatively high comprised between 65 and 75 g, due to the required geometry of specimens for thermal shock testing in the burner rig. The recorded mass change however was not larger than only 0.06 g for the most severe mass change (GBS-TC), which therefore compromises the precision of mass change values as well. Third, the samples were inserted into allocated pockets into the ceramic samples' holder so that only about 1 mm actually emerged over the plate (Figure 2). To fill the gap and somewhat seal samples into place, each cylindrical specimen was wrapped into insulating glass wool stripes approximately 1 mm thick. This design favors heat transfer along the specimen's height to approach operation conditions, though in turn leads to inhomogeneous surfaces exposure to heat and possible associated oxidation. Fourth, quenching tubes made of a heat resistant Co-based alloy are heavily solicited due to high temperatures and frequent blasting quenching air (note the quenching tubes are bent in Figure 2). For this reason, these were protected by thick glass wool socks and further insulated at the base and the end by glass wool stripes maintained by highly reactive iron wires. These wires were heavily oxidized during tests and often replaced together with the wool stripes, both representing possible sources of contamination of the surfaces of specimens. Fifth, mass change in particular to appreciate oxidation is often more appropriately given in $\text{mg}\cdot\text{cm}^{-2}$ as opposed to % in order to take into account the actual surface open to oxidation. In addition to previous considerations, the significant roughness characteristic of materials produced by LPBF may play an important role. Finally, as mentioned earlier, the temperature was not homogeneous within the chamber with gradient of temperatures as high as 100 °C, in particular between the back and front sides of the

combustion chamber due to the machine design. These considerations must be taken into account throughout the manuscript, for all results.

In spite of the abovementioned provisions, the results in Figure 4 were conclusive: each pair of specimens exhibited similar behavior consistently within uncertainty levels. The behaviors of both as-built NiCrAlY-coated Alloy 625 samples were nearly identical (AB in Figure 4). The mass gain was only positive (Figure 4(a)) which indicated the integrity of the NiCrAlY bond coat despite cumulative aggressive thermal shocks. The mass gain increased early by about 0.005 to 0.007 % (approximately 3 to 5 mg) and the weight of specimens remained relatively constant afterwards. The initial mass gain may reasonably be attributed to light oxidation of the specimens and/or possible deposition of impurities from the environment as aforementioned. Despite the relatively high temperatures, the test in burner rig is designed to promote thermal shock and the actual time spent at high temperatures is relatively short. With reference to the thermal cycles in Figure 3, the time spent over 600 °C (where oxidation of Alloy 625 becomes significant [7]) during a typical cycle was only about 5 minutes and time spent over 900 °C was only about 4 minutes (Figure 3(c)). Considering the much longer first cycle for every session (Figure 3(b)), a rough estimation indicates that specimens spent in total less than 50 h above 600 °C and only slightly over 30 h above 900 °C. In a previous publication [7], the oxidation behavior of similar as-built NiCrAlY-coated Alloy 625 samples exhibited rapid initial oxidation of mixed Cr₂O₃ / Al₂O₃ oxides layer within the first few hours of exposure at 900 °C before the mass gain rate decreased significantly, which is in good agreement with the present behavior (note also the rapid color change in Figure 4(b)). Even considering the actual temperatures for each sample, which was as high as 1000 °C for an AB specimen for example, the time spent at high temperature was short. The good oxidation resistance of the system and the relatively short exposure time at high temperatures suggest that oxidation is very limited in the present experimental procedure as

opposed to the dominant effect of rapid heating and cooling cycles which, in fact, promote thermal shock.

Contrary to the as-built materials, specimens coated with the $ZrO_2(Y_2O_3)$ ceramic exhibited weight loss (negative Δm in Figure 4(a)) as a result of thermal cycling. This is typical of TBC systems where the integrity of the ceramic top coat is challenged and significant spallation of the oxides occurs. This is clear by confronting weight loss in Figure 4(a) and top coat external surface aspects in Figure 4(b). As for as-built, each pair of specimens exhibited similar behavior. Both as-built NiCrAlY-coated Alloy 625 with ceramic top coat (AB-TC) exhibited a relatively constant and moderated weight loss (approximately $5 \cdot 10^{-5}$ %/cycle) matching the progressive degradation and spalling of the top coat. It is remarkable that despite the not standardized test carried out associated with unequal quenching and temperature profiles, both specimens exhibited very similar behavior. For the most part, severe spallation of the ceramic top coat, to the point of total removal in certain areas, was pronounced at the edge of the specimens, more so on the side facing the flame at the center of the combustion chamber (note that all macrographs in Figure 4(b) were oriented to face the flame at the bottom of the figure). The behavior of the NiCrAlY-coated Alloy 625 specimens subjected to the grain boundary serration treatment and with ceramic top coat (GBS-TC) were less consistent, however showing similar trends. On the one hand, one specimen experienced rapid weight loss within only the first 60 cycles (dotted light grey line in Figure 4(a)) due to spalling of a large chunk of the ceramic top layer facing the flame while the weight loss afterwards was consistent to that of AB-TC samples. On the other hand, the next GBS-TC specimen (solid light grey line in Figure 4(a)) experienced a more constant weight loss with a rate approximately $2 \cdot 10^{-4}$ %/cycle and severe spalling again at the side facing the flame. In both cases, the bond between top coat and NiCrAlY bond coat for GBS-TC samples appeared clearly weaker than that of AB-TC samples. The more rapid degradation of the ceramic top coat

for GBS-TC samples may be attributed to the unavoidable formation of oxides, in particular on the reactive top surface of the NiCrAlY bond coat, as a result of the grain boundary serration treatment despite the flowing Ar shield. The presence of oxides, possibly an inhomogeneous mixture of external Cr_2O_3 and Al_2O_3 or $\text{Y}_4\text{Al}_2\text{O}_9$ oxide [7], might jeopardize the successful adhesion of the top coat onto the bond coat during the consolidation heat treatment. Evidence is needed to confirm such hypothesis, which seems nonetheless reasonable to rationalize the weaker bond between $\text{ZrO}_2(\text{Y}_2\text{O}_3)$ top coat and NiCrAlY bond coat for GBS-TC samples. It will be discussed further in section 3.6. It also remains to be evaluated the case of the grain boundary serration treatment applied *after* the deposition of the ceramic top coat.

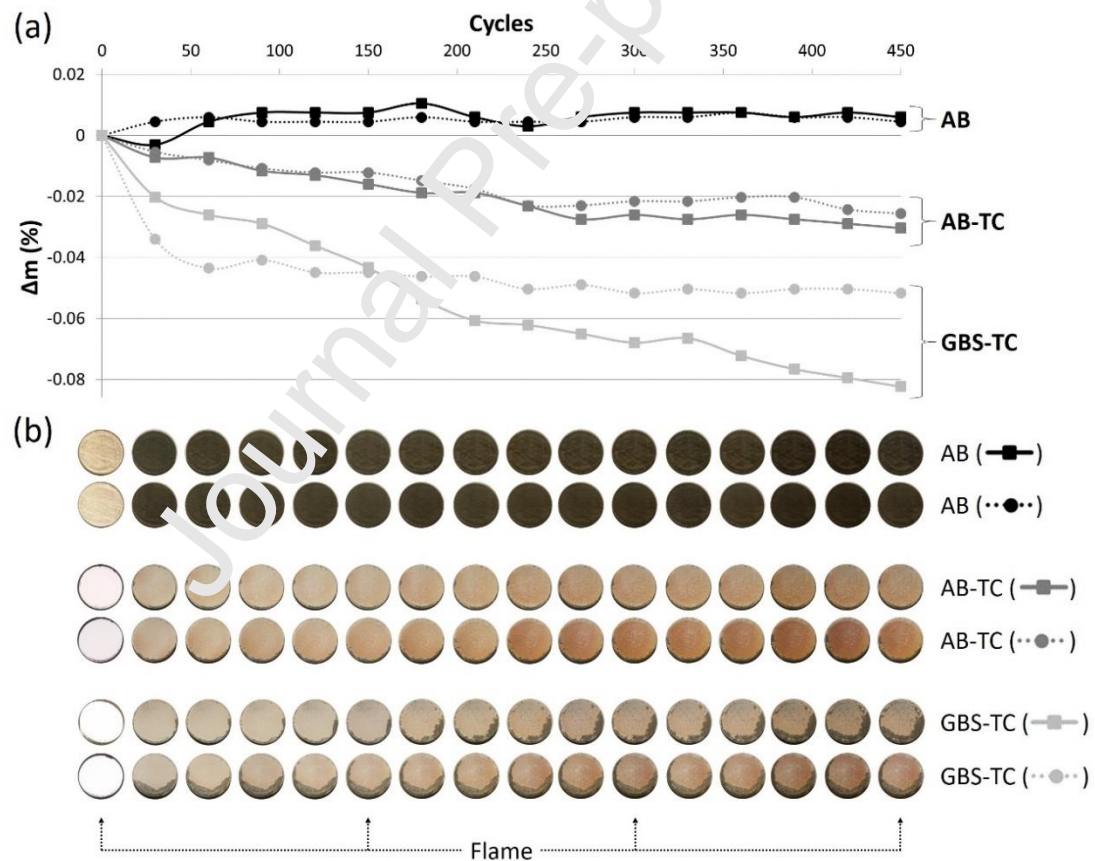


Figure 4: (a) Mass change in %, and (b) corresponding top surface evolution for all six specimens tested as a function of the number of cycles.

Several factors challenge the integrity of ceramic top coats, as listed for example in chapter 13 of [3]. The difference in thermal expansion coefficient between the metallic substrate and the ceramic top coat certainly is significant. This greatly motivates the use of the NiCrAlY bond coat layer, presently processed by LPBF. Transient thermal gradient due to the thermal cycles also contribute to establishing thermal stress into the TBC system. Environmental degradation of the coating may also play a role, though oxidation was limited as previously discussed. The bonding strength between top coat and NiCrAlY bond coat, apparently altered for GBS-TC samples due to heat treatment, perhaps is most critical with regards to spallation. In a previous research [7], the top surface observations of as-built NiCrAlY-coated Alloy 625 similarly produced by LPBF revealed the presence of Y-rich oxides beads between weld tracks and local networks of small cracks. While cracking will be discussed later in section 3.3, it suggests that the surface condition of as-built NiCrAlY-coated Alloy 625, as well as the deposition procedure for the ceramic top coat, should be considered carefully. At last, the effect of quenching in the present experimental procedure may not be discounted. To promote thermal shock and achieve the aggressive thermal cycles in Figure 3, quenching is achieved by small quenching tubes with an internal diameter of approximately 5 mm blowing air at high speed directly onto the specimens surface. Each tube was directed to the center of the top surface of its specimen, with rough precision. While it is difficult to clearly quantify the impact of such direct blow, this certainly added up to the sudden drop in temperature. As mentioned earlier, the similar behavior between each pair of samples was moreover appreciated and brings confidence in the results.

3.2 Cross section analysis

Described in section 2.4, the coating layers profile for each sample condition was investigated. The difficulty to conventionally prepare the samples for observation and testing in cross section, due for the most part to the brittleness and propensity to spallation of the ceramic top coat, is once more accentuated. This suggested in particular that the SolGel process used for depositing the top coat should be appropriately optimized. More conventional methods such as PS or EB-PVD are known to provide better adhesion for the production of TBC systems [3]. Nonetheless, results were fortunately conclusive. Figure 5 compares the cross section for all six conditions: three specimen conditions (AB, AB-TC and GBS-TC) each before (0 cycle) and after (450 cycles) thermal shock test. On the right-hand side in Figure 5, actual cross section optical micrographs of the center portion of each specimen are given (samples were not etched). The NiCrAlY bond coat can be reasonably identified by virtue of the slightly different contrast. The ceramic top coat however had been strapped off the samples due to metallographic preparation, as discussed already. Nevertheless, the thickness of the top coat can be reasonably deducted from the gap between the top surface of bond coats and the mounting resin (and confirmed prior to diamond polishing with cloths). Due to the very small thickness of the TBC systems ($< 400 \mu\text{m}$ approximately) compared to the diameter of specimens ($\approx 22 \text{ mm}$), the thickness of bond coat and top coat were measured every 0.5 mm from edge to edge and schematically presented on the left-hand side in Figure 5. This allowed not only to evaluate accurately the thickness of the different layers all along the specimens, but also to appreciate the layers profiles. The average thickness values measured for each bond coat and top coat are given in Table 3.

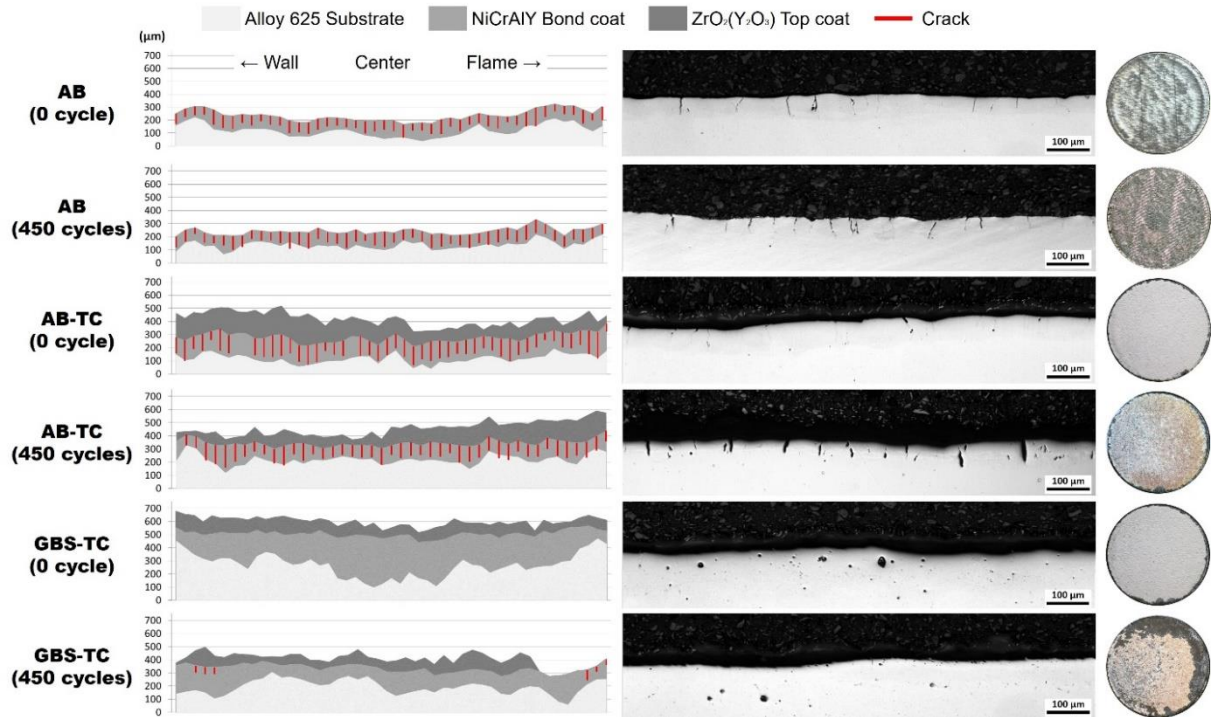


Figure 5: (left) Schematic (whole sample) and (right) optical micrographs with corresponding top surface for all six conditions (AB, AB-TC and GBS-TC after either 0 cycle or 450 cycles).

Table 3: Thickness (in μm) of the NiCrAlY bond coat and $\text{ZrO}_2(\text{Y}_2\text{O}_3)$ top coat layers measured by microscopy in cross section.

		AB	AB-TC	GBS-TC
NiCrAlY bond coat	0 cycle	117 \pm 18 μm	163 \pm 21 μm	236 \pm 72 μm
	450 cycles	105 \pm 19 μm	127 \pm 27 μm	140 \pm 39 μm
$\text{ZrO}_2(\text{Y}_2\text{O}_3)$ top coat	0 cycle	-	139 \pm 44 μm	94 \pm 22 μm
	450 cycles	-	112 \pm 40 μm	69 \pm 31 μm

A number of conclusions can be drawn from these results. Let's consider first the $\text{ZrO}_2(\text{Y}_2\text{O}_3)$ ceramic top coats. It was clear that, despite similar process, top coat deposition on the specimens subjected to the grain boundary serratation heat treatment was less convincing. In Table 3, the average thickness of top coats measured for AB-TC specimens was about 45 μm larger than that

of GBS-TC specimens. As mentioned in section 2.2, the thickness of all top coats measured by eddy current shortly after production was consistent between 137 and 161 μm on average. This suggests that degradation of top coats was unfortunately experienced during travels and manipulations despite great care. This was in particular accentuated due to the bonding and consolidation heat treatment carried out at only 600 $^{\circ}\text{C}$ to preserve microstructure. While it is difficult to evaluate the extent of such degradation, all specimens had been handled together and in a similar way.

With considerations to the NiCrAlY bond coats, there were clear differences between as-built specimens (AB and AB-TC) and those subjected to the grain boundary serration heat treatment (GBS-TC). One effect of the GBS heat treatment, which includes a solutionizing step at 1300 $^{\circ}\text{C}$ for 90 minutes, is the recrystallization of the Alloy 625 substrate [6]. In the present study, the GBS treatment was for the first time applied to the NiCrAlY-Alloy 625 system produced by LPBF. Not only the substrate has recrystallized, as expected [6,10], but the NiCrAlY bond coat also did exhibit a fully recrystallized equiaxed microstructure. This was clear from the results of electron backscattered diffraction (EBSD), highlighted by inverse pole figure (IPF) maps in Figure 6. While as-built AB and AB-TC specimens exhibited the typical columnar grain structure characteristic of powder bed fusion processes (0 cycle in Figure 6), GBS-TC exhibited large equiaxed grains as a result of recrystallization and grain coarsening during heat treatment (the solutionizing step in particular [6]). It is not clear at this stage what this means for the bonding coherence between substrate and bond coat.

In a previous study, the recrystallization of alloys produced by LPBF and subjected to heat treatments was discussed [10]. Such recrystallization is due to the relatively high level of residual stress stored within as-built materials, characteristic of LPBF, which promotes recrystallization by a sole heat treatment providing sufficient temperature is reached (as opposed to usual thermo-

mechanical procedures). Therein, a similarly yet differently built Alloy 625 was found to fully recrystallize after 1 h at 1150 °C. On the other hand, annealing for 1 h at 980 °C, a temperature closer to those involved in the present study, showed no sign of recrystallization (yet?). Several considerations must be made: the actual time spent at high temperatures (discussed earlier when discussing oxidation), the actual temperature profile for each specimen (the maximum temperature plateau for AB, AB-TC and GBS-TC in Figures 6 was approximately 925, 970 and 1000 °C, respectively), the presence of the insulating top coats and their actual thickness and consistency, stress effect of thermal shocks and stress relieving effect of temperature, etc. The temperature range and timing in the frame of the present thermal shock protocol may very well be within the regime of recrystallization for the alloy system considered. Marchese et al. [11] for example observed signs of recrystallization after a similar LPBFed Alloy 625 was subjected to 980 °C for 2 h. Clear evidence lack in the present study to conclude with certainty. The IPF maps of AB and AB-TC after 450 cycles however suggest not to discount recrystallization.

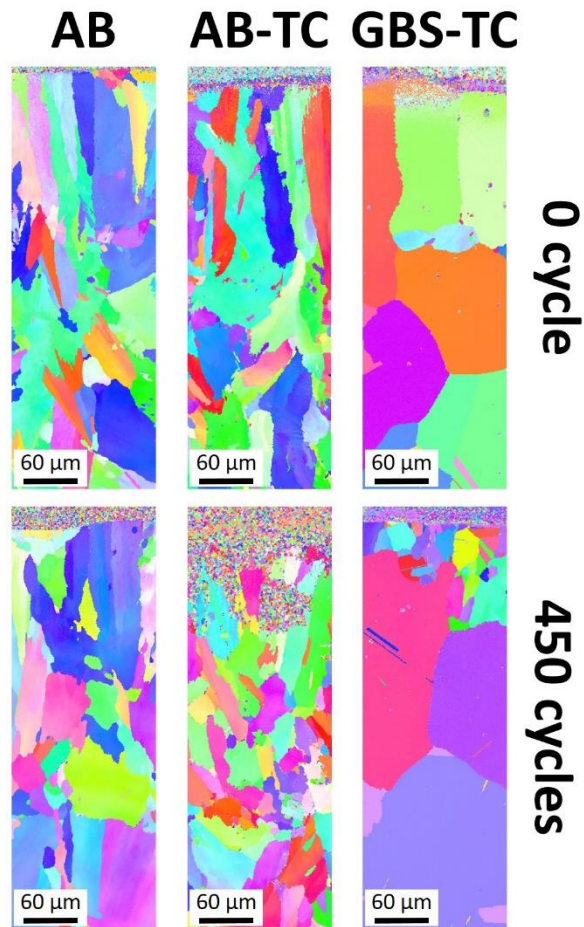


Figure 6: Electron backscattered diffraction (EBSD) inverse pole figure (IPF) maps for all six conditions (AB, AB-TC and GBS-TC after either 0 cycle or 450 cycles) highlighting grains structure.

On the left-hand side in Figure 5, the thin coating layers for each specimen are sketched to appropriate scale for discussion and the measured thickness are given in Table 3. It should be noted that an accurate determination of the interface between Alloy 625 substrate and NiCrAlY bond coat is not easy due to the “dilution zone” inherited from LPBF. As opposed to clearly distinct interface in other deposition methods (APS or EB-PVD for example), this gradual interface is due in particular to the remelting of underlying material during the process [2]. IPF

maps in Figure 6 support this claim. With all precautions, the thickness of the LPBFed deposited bond coat was rather consistent between specimens. The thicknesses measured presently were reasonably in line with those observed during the preliminary process optimization campaign: between 100 and 350 μm thick including the dilution zone, precisely 242 μm at 36 % dilution with 250 W and 800 mm/s [2]. Most importantly, thickness measured on samples after 450 cycles were hardly smaller than their as-built counterpart's which indicated insignificant deterioration of the bond coats. While it is hard to conclude with certainty, the integrity of LPBFed NiCrAlY bond coats appeared unchallenged.

3.3 Cracking within bond coats

In Figure 5, the cross-section micrographs revealed significant cracking of the bond coat normal to the coating. Presence of cracks was probed every 0.5 mm along the width of each sample and included in the schemes by red lines. In addition, the total number of cracks corresponding to each sample's cross section was counted, and the length of each crack was measured (Figure 7). Cracking as a result of LPBF processing is not at all uncommon due to the residual stress development mentioned earlier. The so-called weldability of materials is often considered to account for their processability by LPBF [12]. For example, LPBF of high- γ' superalloys or TiAl intermetallics is very challenging. While the processability of NiCrAlY is also challenging, with more than 9 wt.% Al (Table 1), successful production of crack-free specimens has been demonstrated [2]. It should be noted at this early point that cracking of the bond coat was not observed after LPBF production. While such severe cracking was not anticipated and therefore not focused on, there was no clear signs of cracking on the surface of specimens during

manipulation and testing. Significant cracking was however observed and discussed for similar NiCrAlY-coated Alloy 625 specimens tested for oxidation resistance [7].

From Figures 5 and 7, several conclusions were clear. First, while cracking was relatively severe for as-built specimens (AB and AB-TC in Figures 5 and 7(a)), specimens subjected to the GBS heat treatment clearly exhibited much lower cracking density (GBS-TC in Figures 5 and 7(a)). Second, among as-built specimens, the cracking density was apparently significantly lower for specimens that had been coated (AB-TC) compared to naked specimens (AB). Third, cracks were exclusively observed within the NiCrAlY bond coat and not within the Alloy 625 substrate. This was clear in Figure 7(b) where the average length of cracks was in all cases smaller than the associated average bond coat thickness. More precisely, not a single crack was found to propagate into the substrate. Fourth, the effect of thermal shock cycling was not clear (0 cycle vs. 450 cycles in Figures 5 and 7). In Figure 7(a), more cracks were observed after 450 cycles for both AB-TC and GBS-TC but not for AB specimens. While cracking can be expected as a result of the aggressive thermal shock cycling imposed, no conclusion can be drawn due to the analysis procedure. Crack propagation was also not clear. In Figure 7(b), the gap between cracks length and bond coat thickness decreased after 450 cycles, suggesting that cracks might have propagated further through the coating. The present results do not however authorize clear conclusions. What is very clear, nevertheless, is that specimens conditions (AB, AB-TC or GBS-TC) were definitely more responsible for cracking than thermal shock cycling (0 cycle vs. 450 cycles).

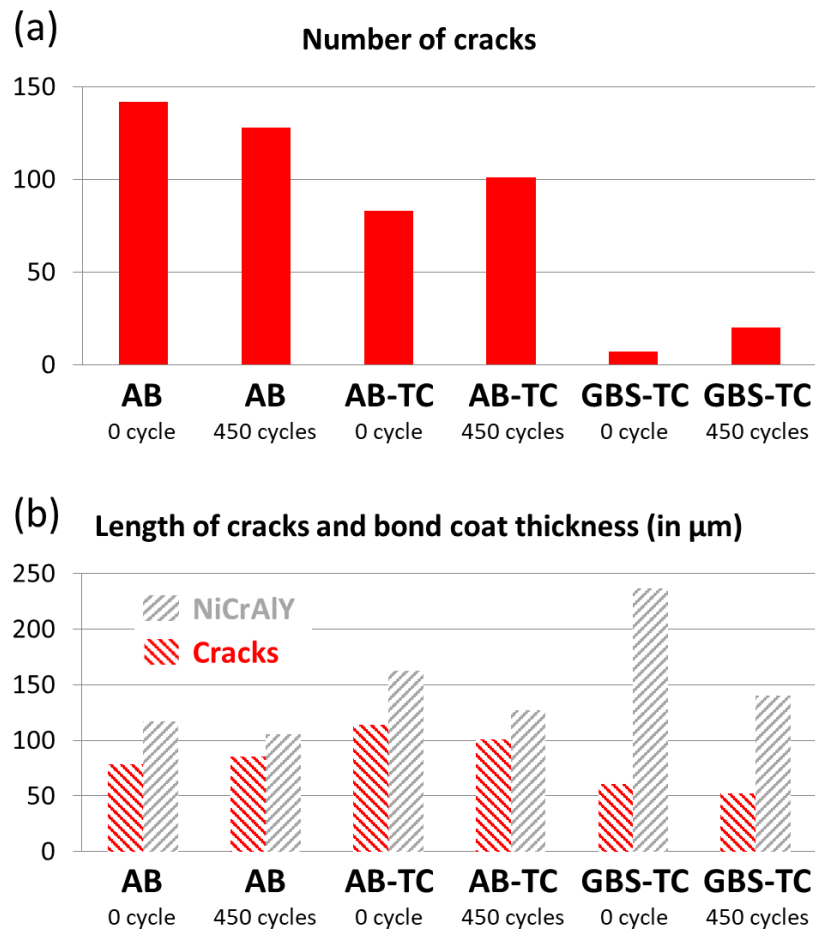


Figure 7: (a) Number of cracks, and (b) average length of cracks and bond coat thickness measured in cross section for all six conditions.

In an attempt to provide an explanation for the cracking of the bond coat, it seems more appropriate to consider samples conditions, in particular the history of the experimental procedure. All nine base specimens were produced at the same time following the procedure described in section 2.1: all nine Alloys 625 22x22 mm² specimens followed by the deposition of two 50 μm NiCrAlY coating layers were produced by LPBF, in France [2]. Three specimens were then shipped to Italy for being subjected to the GBS heat treatment. These were subsequently shipped back to France for the Sol-Gel deposition of the $\text{ZrO}_2(\text{Y}_2\text{O}_3)$ ceramic coating on all six AB-TC and GBS-TC samples, including the low temperature bonding heat treatment (600 °C for 4h). All

nine samples were finally shipped back to Italy for being tested in burner rig. At last, all materials characterizations were carried out in Korea, several months later. Approximately 6 to 8 months had passed between LPBF production and samples characterization, approximately 3 months between LPBF production and thermal shock cycling in burner rig.

The authors reasonably attribute the cracking of NiCrAlY bond coat to the phenomenon known as delayed cracking. With time the significant residual stress stored within the material releases, sometimes to the point of causing parts to crack even at rest. This is one of the reasons why LPBF manufacturers suggest stress-relieving treatments post-production (often 870 °C for 1 h). While it has not been clearly documented to our knowledge, “popping” of LPBFed titanium parts for example is heard occasionally in some laboratories. Delayed cracking is mostly encountered in steel metallurgy and welding. In the present context, it seems reasonable to assume that different levels of stress relieve (therefore interrupting cracking) were experienced by the different specimens. GBS-TC specimens had been relatively early subjected to the GBS heat treatments which promotes full recrystallization thereby relieving all residual stress. This is consistent with the very low cracking density observed on both GBS-TC samples (Figures 5 and 7). On the other hand, AB 0 cycle had never been exposed to heat, not even during thermal shock cycling as for AB 450 cycles. As a matter of fact, the highest number of cracks was found for the AB 0 cycle specimen (Figure 7(a)).

AB-TC specimens had been exposed to 600 °C for 4 h as part of the top coat deposition process, to consolidate the top coat. In a recent publication [10], a similar Alloy 625 (not NiCrAlY) produced by LPBF had been subjected to 600 °C for 1 h and the effect on residual stress levels was investigated. The results did not highlight any effect of such treatment, as opposed to more conventional treatments at higher temperature. It is not clear presently to what extent the top coat bonding treatment contributed to stress relieving of the NiCrAlY bond coat. The total counted

number of cracks in AB-TC specimens was lower than AB specimens in both cases (AB-TC 0 cycle and AB-TC 450 cycles in Figure 7(a)). This suggests that applying a stress relieving treatment just after LPBF production may significantly reduce risks of cracking. Considerations for the GBS heat treatment, for which recrystallization is crucial, should be accounted.

The results of the present study are not appropriate to go beyond conjectures. Attributing the severe cracking observed in as-built specimens to delayed cracking due to large residual stress inherited from LPBF seems nevertheless reasonable. An experimental protocol to account for delay cracking in such specimens seems straight-forward. Applying recrystallization heat treatments (1150 °C for 2 hours for example [13]) to a set of specimens, at different times after production, seems appropriate. The present results suggest that a few months are sufficient to produce significant cracking in as-built specimens, should delay cracking be in facts responsible. At present, it seems inappropriate to further discuss cracking as the effect of thermal shock cycling may likely be clouded.

3.4 Hardness

Vickers microhardness profiles were generated for all specimens, measured from the top of the NiCrAlY bond coat deep into the Alloy 625 substrate. Results for three positions and the resulting average (mean) are displayed in Figure 8. In addition to microhardness profiles, schematics of each specimen in cross section were included (according to the bond coat thickness measured in Table 3). At first glance, microhardness profiles in Figure 8 fit appropriately to expectations and are discussed in the following.

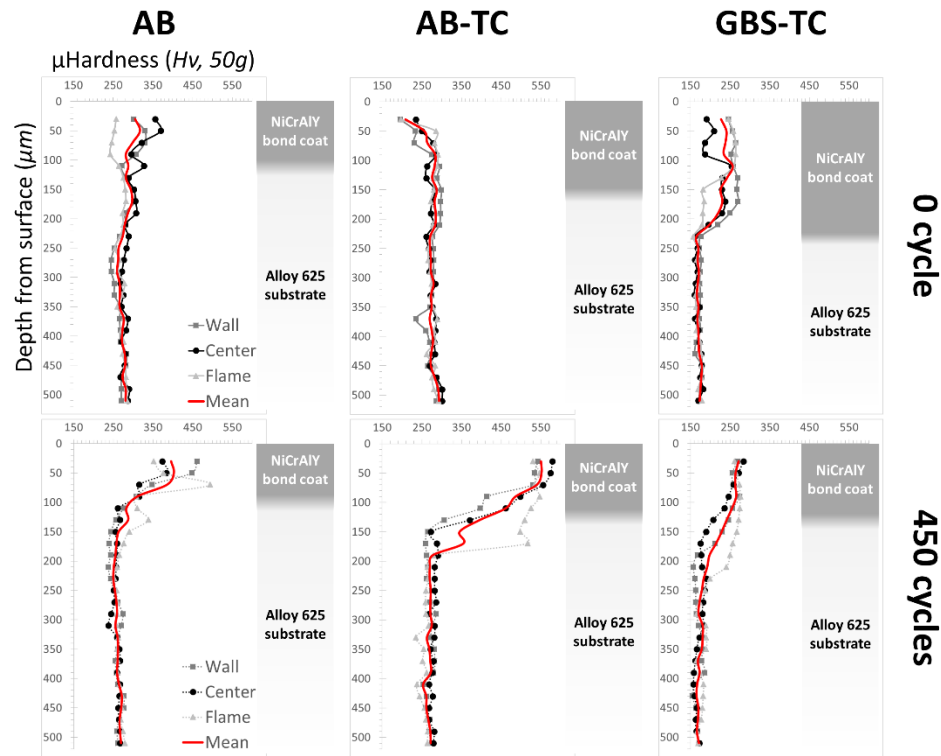


Figure 8: Vickers microhardness (50g) measured every 20 μm from the top surface of the bond coat deep into the substrate. Three series of measurements were carried out: one at the center of the specimen (Center), and one 5 mm away from the center on each side (Flame side vs. furnace Wall side). The average of the 3 values were plot in red (Mean). Schematics of the cross section according to Table 3 were included for each condition.

As per the testing procedure design, only a thin volume of the samples appeared affected by thermal shock cycling, at least regarding thermal aging: for all specimens, the microhardness values were consistent below 250 μm deep into cylindrical specimens. It is reminded that specimens were inserted into apposite sockets through a thick refractory ceramic plate so that only a thin top portion emerged, open to the flame (Figure 2). This is particularly relevant for as-built specimens (AB and AB-TC in Figure 8). As-built LPBFed microstructures are more often than not characterized by very high dislocation density, as for Alloy 625 in particular, indicator of

the high residual stress levels already mentioned [10]. Similar to strain hardening processes, higher dislocation density corresponds to higher hardness. Consistent microhardness profiles after 450 cycles for as-built specimens (AB and AB-TC, 450 cycles in Figure 8) within the Alloy 625 substrate indicate that heat was not sufficient to release stress so as to alter hardness. The microhardness values in the Alloy 625 substrate was consistent for all as-built specimens with an average of $\mu\text{Hv} = 270 \pm 6$. On the other hand, specimens subjected to the GBS heat treatment exhibited significantly lower values with an average of $\mu\text{Hv} = 172 \pm 1$. This is consistent with full recrystallization and grain coarsening experienced during the heat treatment (Figure 6) [6].

Microhardness profiles within the NiCrAlY bond coat of as-built specimens (AB and AB-TC in Figure 8) were consistent with the Alloy 625 substrate at 0 cycle. Note that hardness was evaluated during the microstructural characterization campaign, much later after production, on specimens presenting severe cracking (Figure 5). The discrepancy observed for AB 0 cycle could possibly be attributed to the inhomogeneous microstructure and composition inherited from LPBF [6]. However, inhomogeneity such as crystalline defects density may be felt at relatively lower scale than the three selected locations distant 5 mm. The notably lower microhardness within the first 100 μm of the bond coat in AB-TC 0 cycle could possibly be explained by the top coat bonding treatment at 600 °C for 4 hours. However, the effect of 1 h at this temperature was recently found insignificant with regard to residual stress levels and microstructural healing [10]. Microhardness within the NiCrAlY bond coat for GBS-TC 0 cycle in Figure 8 was clearly higher than that of the substrate for as-built specimens, however lower than those of as-built counterparts. Lower hardness within bond coats after GBS heat treatment may also be explained by recrystallization and grain coarsening (Figure 6). The temperature profile characterizing the GBS heat treatment suggests significant precipitation of γ' in particular [14], which is consistent with greater hardness as compared to the low-Al Alloy 625 substrate.

While thermal shock testing had no significant effect on the substrate, as discussed previously, clear hardening of the NiCrAlY bond coat was observed in Figure 8. GBS-TC 450 cycles exhibited a microhardness profile fairly similar to that of GBS-TC 0 cycle, which testifies of the stability of the fully recrystallized GBS microstructure. On the contrary, both as-built samples experienced significant hardening of the bond coat. It should be reminded at this point that different specimens were studied for the 6 different conditions in all figures. In other words, while similarities may reasonably be accepted, hardness profiles at 0 cycle in Figure 8 do not necessarily match hardness of 450 cycles samples before thermal shock cycling. Highlighted by the profiles at the three different locations considered (Flame, Center and Wall in Figure 8), the discrepancy between microhardness values within bond coats, as high as $\Delta\mu\text{Hv} \approx 100$, imposes to be cautious. Nevertheless, the consistently increasing microhardness profiles within bond coats in as-built specimens after 450 cycles (AB and AB-TC, 450 cycles in Figure 8) brings confidence with regards to the effect of thermal shock cycling.

3.5 Temperature profiles

The theoretical temperature profiles for the TBC systems presently considered can easily be computed. Heat transfer science is robust and well documented, for example in [15]. The heat transfer through the cylindrical specimens can be expressed as:

$$\dot{Q} = \frac{\Delta T}{R} \quad (1)$$

Where \dot{Q} is the rate of heat transfer (in $\text{W}\cdot\text{m}^{-2}$), $\Delta T = T_{TC,BC} - T_s$ is the temperature drop between the top surface of specimen (TC for AB-TC and GBS-TC specimens, BC for AB) and

the bottom surface of the substrate S . These temperatures were set to 950 °C and 300 °C, respectively.

R is the thermal resistance of the system. It can be expressed as:

$$R = R_{TC} + R_{BC} + R_S \quad (2)$$

Where $R_i = \frac{t_i}{A\lambda_i}$ is the thermal resistance of the top coat, bond coat and substrate (i : TC , BC and S , respectively).

$A = 15.2 \times 10^{-4} \text{ m}^2$ is the exchange surface area of 22 mm diameter.

λ_i is the respective thermal conductivity of TC , BC and S : $\lambda_{TC} = 1 \text{ W.m}^{-1}.\text{K}^{-1}$ for a plasma-sprayed YSZ (Y_2O_3 stabilized ZrO_2) [4,16-19], $\lambda_{BC} = 15 \text{ W.m}^{-1}.\text{K}^{-1}$ for a plasma-sprayed NiCrAlY [18] and $\lambda_S = 20 \text{ W.m}^{-1}.\text{K}^{-1}$ for Alloy 625 [20,21].

t_i is the respective thickness of TC , BC and S . The average $\text{ZrO}_2(\text{Y}_2\text{O}_3)$ top coat thickness for the as-coated specimens, measured by eddy current, was $t_{TC} = 145 \text{ }\mu\text{m}$. The NiCrAlY bond coat thickness, averaged for all size specimens in Figures 5 and 7(b) including GBS-TC, was $t_{BC} = 148 \text{ }\mu\text{m}$. Alloy 625 at last was 22 mm thick (Figure 1).

Figure 9 shows schematics for theoretical specimens. The corresponding rate of heat transfer for the system was calculated with equation (1) at $\dot{Q}_{(a)} = 891 \text{ W.m}^{-2}$ in absence of top coat (Figure 9(a)) and $\dot{Q}_{(b)} = 788 \text{ W.m}^{-2}$ with top coat (Figure 9(b)). The temperatures $T_{TC/BC}$ and $T_{BC/S}$ corresponding to the interface between top coat/bond coat and bond coat/substrate, respectively, can be determined by [15]:

$$\dot{Q} = \frac{T_{TC} - T_{TC/BC}}{R_{TC}} \quad (3)$$

$$\dot{Q} = \frac{T_{TC} - T_{BC/S}}{R_{TC} + R_{BC}} \quad (4)$$

Using electrical analogies, the temperature drop ΔT_i within a layer i can also be expressed by:

$$\frac{\Delta T_i}{\Delta T} = \frac{R_i}{R} \quad (5)$$

Computation of equations (1) through (5) indicated that a 145 μm $\text{ZrO}_2(\text{Y}_2\text{O}_3)$ top coat generates a temperature drop of 75 $^\circ\text{C}$ (Figure 9(b)). This highlights the well-known insulation provided by such thermal barrier coating. On the contrary, temperature drop associated with a 148 μm NiCrAlY bond coat was only 5 $^\circ\text{C}$ to 6 $^\circ\text{C}$ (Figures 9(a) and 9(b)). With a Ni-Cr base composition similar to the base metal, the primary function of bond coat such as NiCrAlY is to accommodate thermal expansion misfit between metallic substrate and ceramic top coat [3,4] as well as to provide oxidation resistance [7].

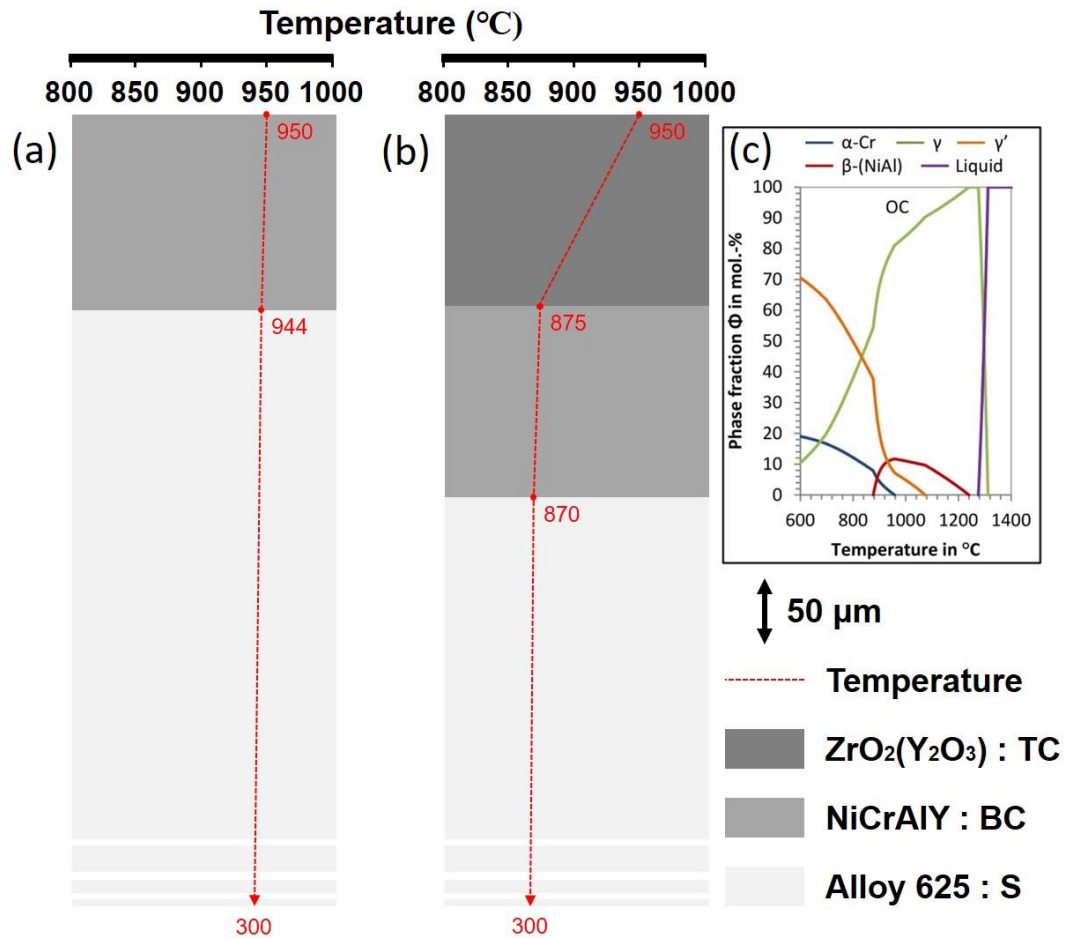


Figure 9: Theoretical temperature profiles for a NiCrAlY-coated Alloy 625 system (a) without and (b) with a ZrO₂(Y₂O₃) thermal barrier. (c) Thermodynamic calculation corresponding to NiCrAlY proposed by Schab et al. [14].

In Figure 9(c), the property diagram for a NiCrAlY coating produced by modular HVOF-spraying published by Schab et al. [14] is reproduced. The temperature range experienced by NiCrAlY bond coats in each specimen at the highest temperature during thermal shock cycling (Figure 3) can widely be comprised between 800 °C and 1000 °C. From Figure 9(c), this clearly falls within significant γ' precipitation. The theoretical temperature profiles in Figures 9(a) and 9(b) only provide so much information: they do not account for inhomogeneous temperature

distribution within the burning chamber (section 2.3), inhomogeneous top coats and bond coats thickness within specimens as well as from one specimen to the other (Figures 5 and 7, Table 3) or degradation of the $ZrO_2(Y_2O_3)$ top coat during testing (Figure 4), to name the most representative. In addition, the theoretical model in Figure 9 portrays the behavior of a “standard” TBC system. However, both the Alloy 625 substrate and the NiCrAlY bond coat were innovatively produced by LPBF. Moreover, the conventional SolGel process used for deposition of the top coat was not optimized, as mentioned in section 2.2. It is beyond the scope of the present investigation to provide more details regarding temperature profiles, precipitation and thorough characterization of resulting microstructures. Experimental procedures more appropriately designed for such purpose are preferable. Nevertheless, elements of the microstructure characterizing the TBC systems studied presently are discussed in the following section 3.6.

3.6 Microstructure

LPBF is known to produce peculiar microstructures due to the characteristics of the process [1,2,6]. As-built microstructures are often anisotropic and inhomogeneous, characterized by a very fine and heavily segregated cellular/dendritic structure. Severe inhomogeneous residual stress levels also define as-built parts. Deviations in microhardness results in Figure 8 highlight these attributes. For this reason, studying presently the microstructure of AB, AB-TC and GBS-TC specimens is difficult to appropriately account for all parameters influencing it. Most relevant factors include the LPBF process which is still challenging for the innovative production of a NiCrAlY-coated Alloy 625 system, the different heat treatments and the inhomogeneous temperature profiles during thermal shock testing. As discussed previously in section 3.3, the

experimental protocol schedule may also be significant with regards to stress release (including delayed cracking in particular). Finally, it is reminded once more that different specimens were used to investigate each condition. Nonetheless, despite limited resolution of SEM-EDS, analyses on cross sections provided valuable clues to refine conclusions.

The microstructure for all as-built Alloy 625 substrates (AB and AB-TC), regardless of the condition (0 cycle and 450 cycles), was consistent with microhardness results previously discussed in section 3.4. All as-built Alloy 625 microstructures were characterized by a very fine cellular/dendritic structure with grains intercepting several melt pools elongated along the building direction, inhomogeneous distribution of the constituting elements, high dislocations density particularly within the interdendritic regions and the presence of very fine Nb and C rich precipitates. Representative high magnification SEM micrographs for all as-built Alloy 625 substrates (AB and AB-TC) are shown in Figure 10. On the contrary in Figure 10, the representative microstructure of Alloy 625 substrates subjected to the GBS heat treatment (GBS-TC) exhibited fully recrystallized equiaxed coarse grains and a relatively large amount of coarser inter and intragranular precipitates, all identified by EDS as niobium carbides NbC. This is consistent with a previous study detailing the design and characterization of the GBS heat treatment for LPBFed Alloy 625 [6]. The effect of the GBS heat treatment was by far the most significant and is consistent with microhardness results presented in Figure 8. As-built Alloy 625 substrates (AB and AB-TC) exhibited high hardness due for the most part to the constrained cellular/dendritic microstructure characterized by high dislocations density and very fine precipitation. Conversely, the fully recrystallized GBS microstructure displayed significantly lower microhardness in Figure 8. Figure 10 shows the representative SEM micrographs for substrates in the vicinity of the NiCrAlY interface, before and after thermal shock cycling (0 and 450 cycles, respectively). Substrates showed no significant difference between 0 and 450 cycles

specimens, besides an apparently more extensive precipitation. With reference to the theoretical thermal profiles generated in Figure 9 and the time-temperature transformation (TTT) diagram of Alloy 625 [10], it is reasonable to assume that the considered volume of material may be exposed to temperatures comprised between 900 °C and 750 °C for sufficient time to promote the precipitation and growth of carbides. It could be speculated from Figure 8 that the as-built substrate closest to the bond coat interface may have experienced notable hardening after 450 cycles, however with little more than suspicions. More thorough analyses of the microstructure are needed to appropriately provide conclusions.

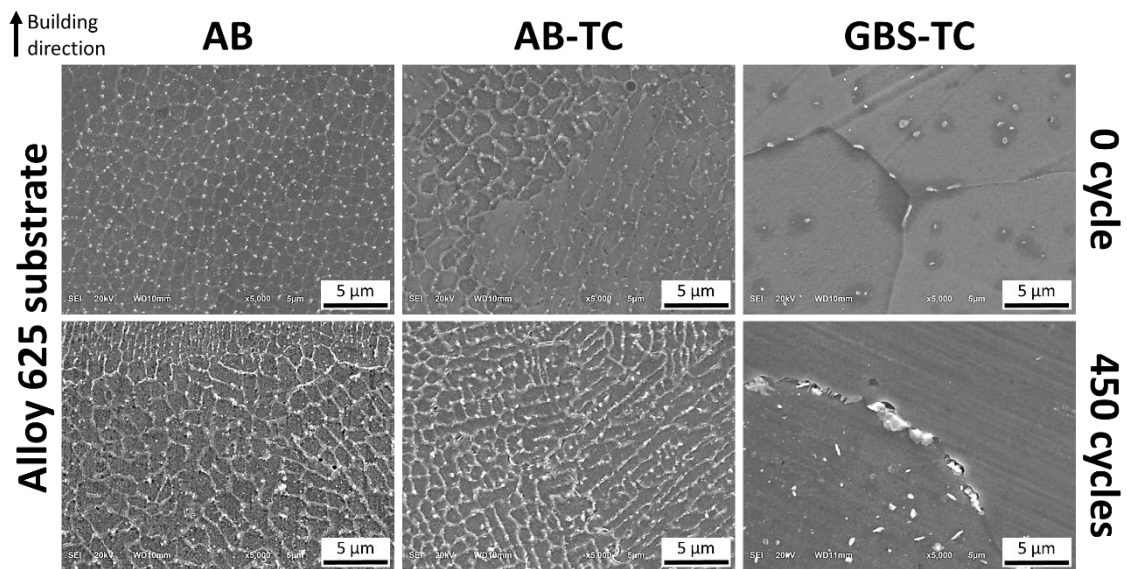


Figure 1: Representative SE-SEM micrographs of the Alloy 625 substrate in as-built conditions (AB and AB-TC) and after grain boundary serration heat treatment (GBS-TC) before (0 cycle) and after (450 cycles) thermal shock cycling. Only the Ni-based γ matrix and Nb-rich MC carbides were clearly detected.

The effect of the GBS heat treatment was also most significant considering NiCrAlY coatings. The microstructure exhibited by NiCrAlY bond coats of as-built specimens (AB and AB-TC, 0

cycle) was similar to that of the Ni-Cr base Alloy 625. In Figure 11, representative SEM micrographs of the as-built NiCrAlY-Alloy 625 interface (AB and AB-TC, 0 cycle) presented a similarly fine cellular/dendritic structure. Inhomogeneous distribution of the constituting elements, high dislocations density and the presence of fine precipitates were also observed. This was consistent with previous studies on optimization of the LPBF process for the innovative production of NiCrAlY-coated Alloy 625 [2] and characterization of its oxidation behavior [7]. This latter publication provides a detailed characterization of the as-deposited LPBFed NiCrAlY bond coat microstructure and constitution. Due in part to some extent of remelting of underlying material during the LPBF process, the chemical composition of NiCrAlY coated deposited onto Alloy 625 was characterized by significant diffusion of the constituting elements leading to gradients of composition much less pronounced compared to conventionally sprayed bond coats. Relatively high contents of Nb and Mo were for example detected within NiCrAlY bond coats. Y was also found to fully segregate to the top [7]. Relatively similar values of microhardness within bond coats at 0 cycle in Figure 8, with respect to the Alloy 625 substrate, suggest similar phase compositions and microstructure. Nevertheless, the large deviations in hardness profiles within bond coat invite to be cautious. More thorough analyses of the LPBFed NiCrAlY microstructure is needed to reject the presence of additional phases such as γ' or σ for example [7]. The characterization of bond coats for specimens including ceramic top coats (TC specimens) was severely challenged by the metallographic preparation mentioned earlier. There was no clear evidence with the presently limited microstructure characterization of the presence of other phases, even after thermal shock cycles. According to the Thermocalc calculation corresponding to NiCrAlY displayed in Figure 9(c) [14], precipitation of the strengthening phase γ' Ni₃Al may be significant during thermal shock cycling. Formation of carbides, from the superalloy reservoir in particular, may also be observed. These considerations are in line with clearly higher hardness

values measured for as-built specimens after 450 cycles in Figure 8. More thorough analyses of the microstructure are again needed to appropriately provide conclusions.

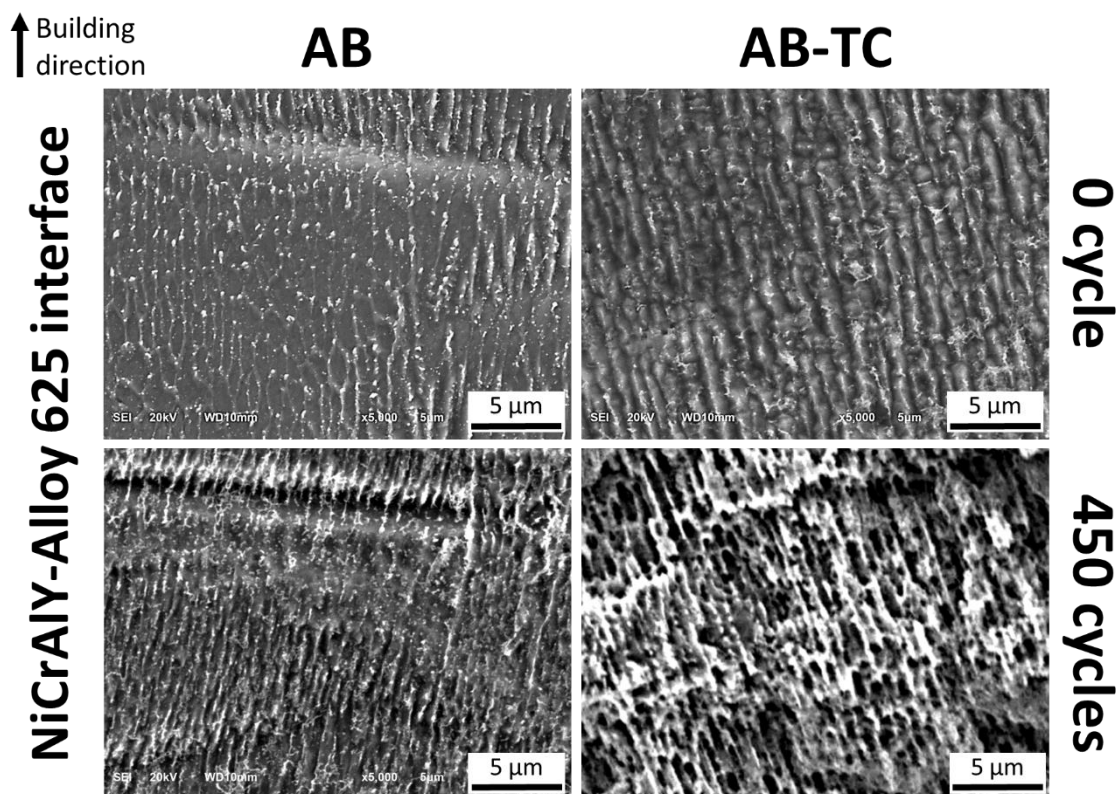


Figure 11: Representative SE-SEM micrographs of the NiCrAlY-Alloy 625 interface region in as-built conditions (AB and AB-TC) before (0 cycle) and after (450 cycles) thermal shock cycling.

Figure 12 shows an SEM cross section micrograph and corresponding EDS element mapping for GBS-TC 0 cycle. Figure 12 highlights several characteristics discussed earlier. First, a cavity was distinctly observed between the Zr-rich top coat layer and the NiCr-rich bond coat. This was caused by large parts of top coats removed during metallographic preparation (which included mechanical polishing) despite all care and highlights the poor bonding between top and bond coats discussed previously (Figure 4). A relatively thick and consistent $Y_4Al_2O_9$ oxide (YAM)

layer was also clearly observed over the top surface of the NiCrAlY bond coat, corresponding to the interface with the $ZrO_2(Y_2O_3)$ top coat. Segregation of yttrium as a result of LPBF had been observed and discussed in [7]. Y was found to fully segregate to the top of specimens, however more specifically between welding tracks. Similar oxides blobs were also observed on as-built specimens AB and AB-TC. However, the YAM layer presently observed for GBS-TC specimens in Figure 12 was clearly more consistent. In section 3.1, the more rapid spallation of the top coat for GBS-TC specimens was possibly attributed to the inevitable formation of oxides during heat treatment despite protective Ar flow. Such consistent YAM layer, not detected in as-built specimens AB or AB-TC and therefore likely promoted by the GBS heat treatment, may well be responsible for the clearly poorer bonding of the top coat for GBS-TC specimens (Figure 4). This should be further investigated as it clearly was detrimental to thermal shock resistance of the TBC system.

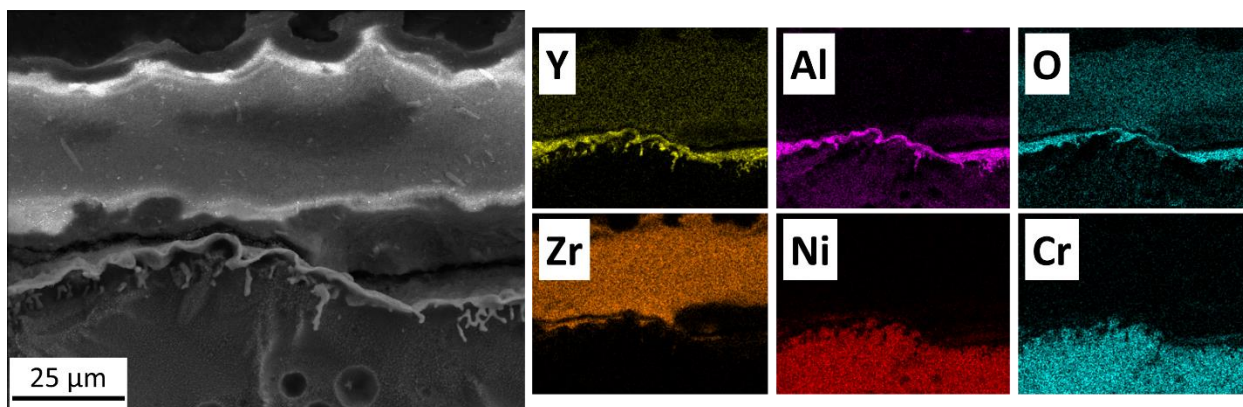


Figure 12: Representative SE-SEM micrographs of the $ZrO_2(Y_2O_3)$ -NiCrAlY interface region in heat treated conditions (GBS-TC) before thermal shock cycling (0 cycle) and associated EDS element mapping.

As for the Alloy 625 substrate, the effect of the GBS heat treatment was tremendous. The microstructure within the GBS-TC NiCrAlY bond coat was fully recrystallized and significant precipitation was clearly observed. Figure 13 shows the microstructure of test specimens, produced in all similar way as thermal shock specimens though in absence of ceramic top coat for easier characterization. This is presently the first time that the proprietary GBS heat treatment is being reported for a NiCrAlY coating produced by LPBF, itself quite unusual. Figure 13(a) displays a relatively low magnification SE-SEM micrograph, associated with element mapping for the major elements considered. Recrystallization is evident and in Figure 13(a), no clear indication of the Alloy 625 substrate and NiCrAlY bond coat interface is observed. EDS element mapping corresponding to the squared area in Figure 13(a) clearly confirms the presence of a relatively thick and consistent $Y_4Al_2O_9$ oxide (YAM) layer discussed previously. Occasional Y segregation relatively deep into the coating was also observed. Despite the large scale of Figure 13(a), EDS element mapping clearly revealed the presence of secondary phases rich either in Cr, Nb or Mo or a combination thereof. As discussed previously, NiCrAlY-coated Alloy 625 produced by LPBF is characterized by a gradient of concentration within a dilution zone due to remelting and thermal history during the process. In fact, relatively high contents of Nb and Mo within LPBFed NiCrAlY bond coats are clear in Figure 13 and were also detected in a previously mentioned study [7].

Micrographs in Figures 13(b) and 13(c), taken at identical magnification, provide indications about phase formation. These phases are most likely a consequence of the GBS heat treatment as these were not observed in as-built materials AB, AB-TC and [7]. As first consideration, depletion of Ni and Al confirms second phase formation. Three clearly distinct phases could be observed in Figure 13(b): Nb-Mo rich, Cr-Mo rich and Mo-rich. Similar observations in Figure 13(c) brings confidence. Several references can be used to estimate the nature of these phases: the

different phases found in superalloys [3] and Alloy 625 in particular [22], the different phases found in NiCrAlY overlay (Figure 9(c) and [3]), the phases observed in NiCrAlY-coated Alloy 625 produced by LPBF [7], experience of the GBS heat treatment for Alloy 625 produced by LPBF [6].

With all precautions due to limited results, some educated speculations can nevertheless be discussed. Note that the iron Fe profile was not conclusive, which decreased the probability of the presence of Laves phase. Ni and Al depletions clearly indicate second phase formation. Cr-rich area could possibly indicate the presence of σ phase (CrNiMo) [3]. The σ phase was identified, with similar morphology, in a similarly produced NiCrAlY-coated Alloy 625 produced by LPBF studied for oxidation resistance however subjected to a different heat treatment of diffusion [7]. The NiCrAlY α -Cr phase is also a strong candidate (Figure 9(c)), expected for NiCrAlY coatings, and was also identified in the abovementioned report [7]. Nb-rich area could indicate the presence of the δ phase (Ni₃Nb) [3]. The Mo-rich area, systematically surrounding these phases as well as within, is more puzzling. Despite the unusual morphologies of these phases in Figures 13(b) and 13(c), carbides may very well be a strong possibility. More specifically Nb-rich MC, Mo-rich M₆C and Cr-rich M₂₃C₆ seem reasonable considering the temperature profile of the GBS treatment (section 2.2 and [6]). At lower scale, highlighted by circles in Figure 13(b), possible evidence of γ' precipitation and σ phase (Mo-rich) or δ phase (Nb-rich) were observed. More thorough analyses of the microstructure are required, beyond the scope of the present report. The above speculations are strengthened by the GBS-TC results of hardness in Figure 8. Despite recrystallization, higher levels of microhardness within coatings at 0 cycle support the precipitation of γ' in particular. This suggests a more stable microstructure of the recrystallized GBS material [6].

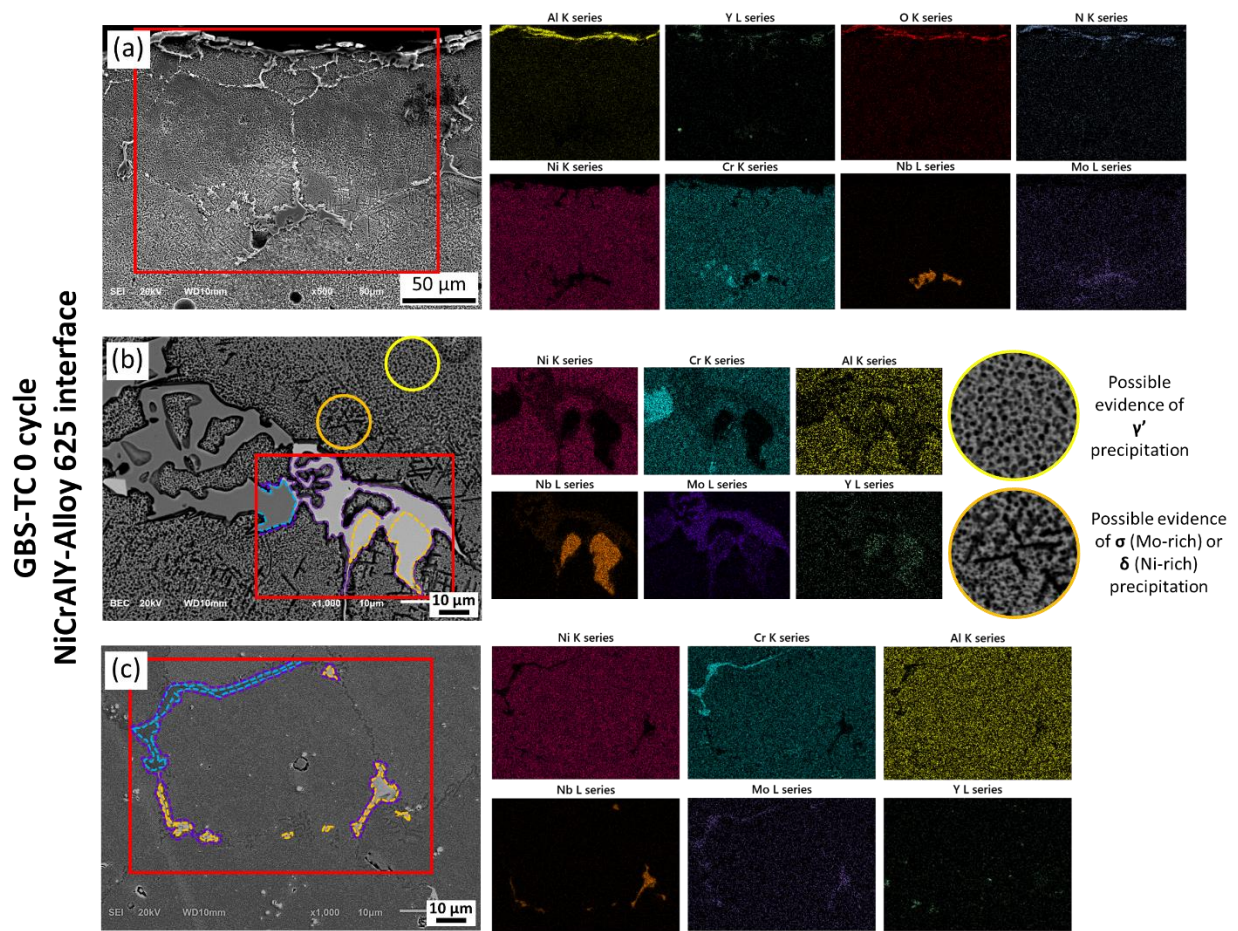


Figure 13: SEM micrographs of the NiCrAlY bond coat region in heat treated conditions (GBS-TC) before thermal shock cycling (0 cycle).

4. Conclusions

A NiCrAlY-coated Alloy 625 was innovatively produced by laser powder bed fusion (LPBF). Test samples including a SolGel ceramic $ZrO_2(Y_2O_3)$ top coat and a specific grain boundary serration heat treatment were subjected to very severe thermal shock cycles between 950 °C and 300 °C designed to render gas turbine conditions. Despite hazardous protocols, a number of conclusions suggest the outstanding potential of LPBF to produce multi-material systems:

1. In spite of severe thermal shock cycling, LPBFed NiCrAlY coatings showed virtually no sign of damage. On the contrary, sprayed ceramic top coats exhibited poor bonding and significant spallation, particularly for heat treated specimens characterized by surface oxidation.
2. Significant cracking was observed within as-built NiCrAlY bond coat, however the source of cracking could likely be attributed to the LPBF processing. Specimens subjected to GBS treatments, fully recrystallized and therefore released of residual stress, exhibited very little cracking.
3. Microhardness profiles and microstructure analysis of as-built specimens suggested precipitation due to heat exposure during thermal shock cycling. On the other hand, the microstructure after heat treatments was found more stable, characterized by large precipitation of relatively stable second phases.

The present study contributes to a series of investigations [2,6,7,10] demonstrating the great potential for manufacturing excellent high temperature structural components by means of LPBF as opposed to more constraining conventional routes.

CRedit authorship contribution statement

Mathieu Ternier: Conceptualization, Methodology, Validation, Formal analysis, Investigation, Data Curation, Writing - Original Draft, Writing - Review & Editing, Visualization, Supervision, Project administration. **Jiwon Lee:** Validation, Formal analysis, Investigation, Data Curation. **Baptiste Ruggieri:** Formal analysis, Investigation. **Etienne Copin:** Validation, Resources, Data Curation, Writing - Review & Editing, Supervision. **Oxana Ostrovskaya:** Resources, Writing -

Review & Editing, Supervision. **Claudio Badini**: Resources, Writing - Review & Editing, Supervision. **Philippe Lours**: Validation, Resources, Writing - Review & Editing, Visualization, Supervision, Project administration, Funding acquisition. **Hyun-Uk Hong**: Validation, Resources, Writing - Review & Editing, Visualization, Supervision, Project administration, Funding acquisition.

Declaration of competing interest

The authors declare that they have no known competing financial interests or personal relationships that could have appeared to influence the work reported in this paper.

Acknowledgment

This research was supported by Changwon National University in 2019~2020.

The authors acknowledge the financial support of the National Research Foundation of Korea (NRF) grant funded by the Korean government (Ministry of Science and ICT/MSIT, NRF-2020R1A2C4002291).

References

- [1] Shaun Cooke, Kevin Ahmadi, Stephanie Willerth, Rodney Herring, Metal additive manufacturing: Technology, metallurgy and modelling, *J. Manuf. Process.* 57 (2020) 978-1003. <https://doi.org/10.1016/j.jmapro.2020.07.025>
- [2] Jiwon Lee, Mathieu Ternier, Etienne Copin, Philippe Lours, Hyun-Uk Hong, A novel approach to the production of NiCrAlY bond coat onto IN625 superalloy by selective laser melting, *Additive Manuf.* 31 (2020) 100998. <https://doi.org/10.1016/j.addma.2019.100998>
- [3] Matthew J. Donachie, Stephen J. Donachie, SUPERALLOYS A Technical Guide, Second Edition, ASM International (2002) 402 pages. <https://doi.org/10.31399/asm.tb.stg2.9781627082679>
- [4] Roger C. Reed, The Superalloys, Fundamentals and Applications, Cambridge University Press (2006). <https://doi.org/10.1017/CBO9780511541285>
- [5] Damien Texier, Daniel Monceau, Zeline Hervier, Eric Andrieu, Effect of interdiffusion on mechanical and thermal expansion properties at high temperature of a MCrAlY coated Ni-based superalloy, *Surf. Coat. Tech.* 307 (2016) 81-90. <https://doi.org/10.1016/j.surfcoat.2016.08.059>
- [6] Jiwon Lee, Mathieu Ternier, Sunyoung Jun, Hyun-Uk Hong, Etienne Copin, Philippe Lours, Heat treatments design for superior high-temperature tensile properties of Alloy 625 produced by selective laser melting, *Mat. Sci. Eng. A* 790 (2020) 139720. <https://doi.org/10.1016/j.msea.2020.139720>
- [7] Damien Texier, Etienne Copin, Agustin Flores, Jiwon Lee, Mathieu Ternier, Hyun-Uk Hong, Philippe Lours, High temperature oxidation of NiCrAlY coated Alloy 625 manufactured by selective laser melting, *Surf. Coat. Tech.* 398 (2020) 126041. <https://doi.org/10.1016/j.surfcoat.2020.126041>
- [8] Justine Fenech, Céline Viazzi, Jean-Pierre Bonino, Florence Ansart, Antoine Barnabé, Morphology and structure of YSZ powders: Comparison between xerogel and aerogel, *Ceram. Int.* 35-8 (2009) 3427-3433. <https://doi.org/10.1016/j.ceramint.2009.06.014>
- [9] Lisa Pin, Vanessa Vidal, Fabien Blas, Florence Ansart, Sandrine Duluard, Jean-Pierre Bonino, Yannick Le Maoult, Philippe Lours, Optimized sol-gel thermal barrier coatings for long-term cyclic oxidation life, *J. Eur. Ceram. Soc.* 34-4 (2014) 961-974. <https://doi.org/10.1016/j.jeurceramsoc.2013.10.013>
- [10] Mathieu Ternier, Jiwon Lee, Giulio Marchese, Sara Biamino, Hyun-Uk Hong, Electron Backscattered Diffraction to Estimate Residual Stress Levels of a Superalloy Produced by Laser Powder Bed Fusion and Subsequent Heat Treatments, *Materials* 13 (2020) 4643. <https://doi.org/10.3390/ma13204643>
- [11] Giulio Marchese, Simone Parizia, Masoud Rashidi, Abdollah Saboori, Diego Manfredi, Daniele Ugues, Mariangela Lombardi, Eduard Hryha, Sara Biamino, The role of texturing and microstructure evolution on the tensile behavior of heat-treated Inconel 625 produced via laser powder bed fusion, *Mat. Sci. Eng. A* 769 (2020) 138500. <https://doi.org/10.1016/j.msea.2019.138500>

- [12] Jamison L. Bartlett Xiaodong Li, An overview of residual stresses in metal powder bed fusion, *Additive Manuf.* 27 (2019) 131-149. <https://doi.org/10.1016/j.addma.2019.02.020>
- [13] Giulio Marchese, Massimo Lorusso, Simone Parizia, Emilio Bassini, Ji-Won Lee, Flaviana Calignano, Diego Manfredi, Mathieu Terner, Hyun-Uk Hong, Daniele Ugues, Mariangela Lombardi, Sara Biamino, Influence of heat treatments on microstructure evolution and mechanical properties of Inconel 625 processed by laser powder bed fusion, *Mat. Sci. Eng. A* 729 (2018) 64-75. <https://doi.org/10.1016/j.msea.2018.05.044>
- [14] J.C. Schab, J.R.A. Zimmermann, P.-D. Grasso, A. Stankowski, S. Heinze, A. Marquardt, C. Leyens, Thermodynamic calculation and experimental analysis of critical phase transformations in HVOF-sprayed NiCrAlY-coating alloys, *Surf. Coat. Tech.* 357 (2019) 924-938. <https://doi.org/10.1016/j.surfcoat.2018.10.057>
- [15] Yunus A Çengel, Heat transfer: a practical approach, Second Edition, McGraw-Hill New York (2004) 908 pages, ISBN: 0071236449 9780071236447
- [16] Ningning Hu, Matiullah Khan, Yongzhe Wang, Xuemei Song, Chucheng Lin, Chengkang Chang, Yi Zeng, Effect of Microstructure on the Thermal Conductivity of Plasma Sprayed Y2O3 Stabilized Zirconia (8% YSZ), *Coatings* 7 (2017) 198. <https://doi.org/10.3390/coatings7110198>
- [17] Pierre Planques, Vanessa Vidal, Philippe Lours, Vincent Proton, Fabrice Crabos, Juliette Huez, Bernard Viguier, Mechanical and Thermo-physical Properties of Plasma-Sprayed Thermal Barrier Coatings: A Literature Survey, *Oxid. Met.* 88 (2017) 133-143. <https://doi.org/10.1007/s11085-016-9693-1>
- [18] Rochelle Brandt, Lech Pawlowski, Günther Neuer, Pierre Fauchais, Specific heat and thermal conductivity of plasma sprayed yttria-stabilized zirconia and NiAl, NiCr, NiCrAl, NiCrAlY, NiCoCrAlY coatings, *High Temp.-High Press.* 18 (1986) 65-77. https://www.researchgate.net/publication/233851641_Specific_heat_and_thermal_conductivity_of_plasma_sprayed_yttria-stabilized_zirconia_and_NiAl_NiCr_NiCrAl_NiCrAlY_NiCoCrAlY_coatings
- [19] Julian D. Osorio, Alejandro Toro, Juan P. Hernandez-Ortiz, Thermal Barrier Coatings for Gas Turbine Applications: Failure Mechanisms and Key Microstructural Features, *Dyna* 176 (2012), 149-158. https://www.researchgate.net/publication/262462690_Thermal_Barrier_Coatings_for_Gas_Turbine_Applications_Failure_Mechanisms_and_Key_Microstructural_Features
- [20] INCONEL[®] alloy 625 brochure, Special Metals. <https://www.specialmetals.com/assets/smc/documents/alloys/inconel/inconel-alloy-625.pdf>
- [21] HAYNES[®] 625 alloy brochure, Haynes International. https://www.haynesintl.com/docs/default-source/pdfs/new-alloy-brochures/high-temperature-alloys/brochures/625-brochure.pdf?sfvrsn=967229d4_26
- [22] Stephen Floreen, Gerhard E. Fuchs, Walter J. Yang, The Metallurgy of Alloy 625, Superalloys 718,625,706 and Various Derivatives, The Minerals, Metals & Materials Society (1994). https://www.tms.org/Superalloys/10.7449/1994/Superalloys_1994_13_37.pdf